PCCP

Atomistic level aqueous dissolution dynamics of NASICON-Type $Li_{1+x}Al_xTi_{2-x}(PO_4)_3$ (LATP)

Journal:	*Physical Chemistry Chemical Physics*
Manuscript ID	CP-COM-11-2021-005360.R1
Article Type:	Communication
Date Submitted by the Author:	30-Dec-2021

Complete List of Authors:	Sengul, Mert; University of Maryland Baltimore, Ndayishimiye, Arnaud; Pennsylvania State University, Materials Research Institute Lee, Wonho; Kumoh National Institute of Technology, ; Seo, Joo-Hwan; The Pennsylvania State University, Department of Materials Science & Engineering Fan, Zhongming; Penn State - Main Campus, Materials Science and Engineering Shin, Yun Kyung; Pennsylvania State University, Mechanical and Nuclear Engineering Gomez, Enrique; The Pennsylvania State University, Chemical Engineering, Materials Science and Engineering Randall, Clive; Pennsylvania State University, Center for Dielectric Studies, Materials Research Institute, University Park, Pa 16802 USA, van Duin, Adri; The Pennsylvania State University, Mechanical and Nuclear Engineering

COMMUNICATION

Atomistic level aqueous dissolution dynamics of NASICON-Type $Li_{1+x}Al_xTi_{2-x}(PO_4)_3$ (LATP)

Received 00th January 20xx,
Accepted 00th January 20xx

DOI: 10.1039/x0xx00000x

Mert Y. Sengul [a, ‡], Arnaud Ndayishimiye [b, ‡], Wonho Lee [b, e], Joo-Hwan Seo [a], Zhongming Fan [b], Yun Kyung Shin [d], Enrique D. Gomez [b, c], Clive A. Randall [a, b] and Adri C. T. van Duin *[,d]

Advancing the atomistic level understanding of aqueous dissolution of multicomponent materials is essential. We combined ReaxFF and experiments to investigate the dissolution at the $Li_{1+x}Al_xTi_{2-x}(PO_4)_3$-water interface. We demonstrate that surface dissolution is a sequentially dynamic process. The phosphate dissolution destabilizes the NASICON structure, which triggers a titanium-rich secondary phase formation.

The world's growing demand on energy and its storage is one of the main drivers of academic and industrial research on clean alternatives. In this regard, advancements in the technology of Lithium-ion batteries (LIB) as electrochemical energy storage devices, with applications ranging from portable devices to high power sources for the automotive industry, are essential in managing the green transition from fossil fuels to clean and renewable alternatives.

Ceramics solid electrolytes are excellent conductors at room temperature. In addition, they are very stable at elevated temperatures, which makes them a promising candidate for LIB applications. Among ceramic-based solid electrolytes, oxides with NASICON-type structure show higher ionic conductivity (~10^{-4} S cm^{-1}) with $Li_{1.3}Al_{0.3}Ti_{1.7}(PO_4)_3$ (LATP) being one of the most promising for envisioned applications [1, 2]. To obtain these high conductivity values, these ceramics must be dense, which can be achieved at high temperatures (~1000 °C) using conventional sintering techniques [3-5]. Several limitations were reported due to the required elevated temperatures for the sintering of these materials, which include but are not limited to the dangerous treatment of the material, high processing costs, low densities and Li-loss in the sintering process. [6-8]. To avoid these limitations, several approaches have been adopted to synthesize LATP at lower temperatures, such as sol–gel [9, 10], solution [6], hydrothermal [11] methods and field-assisted sintering [12] for densification; however, the conductivity values were often compromised during these treatments. The cold sintering process (CSP) has been recently introduced as a non-equilibrium low-temperature sintering method, which uses solvents as a transient phase to enhance grain boundary and surface diffusion [13, 14]. The CSP has been applied to over 80 inorganic materials, including NASICON-type materials, and other important components of Li-batteries [8, 15, 16]. The temperatures are low enough that it has been successfully applied for the sintering of ceramic-matrix composites to enhance physical properties [17-19]. However, similar to other solvent based synthesis techniques, cold sintering of LATP suffers from the incongruency during dissolution when powder is in contact with solvent. The incongruent dissolution of species (i.e., the stoichiometry of dissolution is different from the bulk stoichiometry) is also a common problem for all NASICON-type materials due to the wide variety of chemical bonding and high reactivity with water particularly in the presence of Li-ions [3, 20].

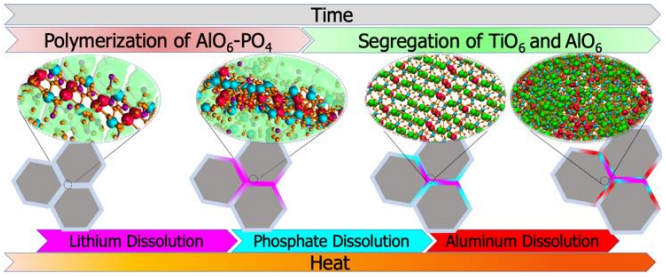

Figure 1. Graphical representation of the incongruent dissolution mechanism observed in this work. The grey pentagons represent the LATP grains. Key: Ti (green); P (cyan); Al (red); Li (purple).

[a.] *Department of Materials Science and Engineering, The Pennsylvania State University, University Park, Pennsylvania, 16802, USA*
[b.] *Materials Research Institute, The Pennsylvania State University, University Park, Pennsylvania, 16802, USA*
[c.] *Department of Chemical Engineering, The Pennsylvania State University, University Park, Pennsylvania, 16802, USA*
[d.] *Department of Mechanical Engineering, The Pennsylvania State University, University Park, Pennsylvania, 16802, USA*
[e.] *Department of Polymer Science and Engineering, Kumoh National Institute of Technology, Gumi-si, Gyeongbuk, 39177, Republic of Korea*
‡ These authors contributed equally.
* Corresponding Author: Adri C. T. van Duin (acv13@psu.edu
Electronic Supplementary Information (ESI) available: [details of any supplementary information available should be included here]. See DOI: 10.1039/x0xx00000x

The dissolution pathways of multicomponent systems in water can be very complex and is difficult to investigate spectroscopically [21]. Current surface science techniques are limited and would require using *ex situ* methods and/or beam line techniques that are complex and not readily accessible in the examination of solid/liquid interfaces at elevated temperatures and pressures. Here we present an atomistic level investigation of dissolution dynamics at the LATP/water interface. This study advances our description of dissolution kinetics of LATP while providing insights on all NASICON-type materials and compositions for both Li and Na based battery technologies. In addition, the dissolution mechanism presented here exemplifies the level of complexity of multicomponent dissociation dynamics. To our knowledge, this is the first atomistic level study that investigates the aqueous dissolution of a NASICON-type material. Here, we revealed a unique dissolution mechanism that can be observed in similar multicomponent chemical systems. Our results show that the dissolution of LATP is a sequential process (Figure 1) and it is not only due to surface protonation, but also triggered by the rapid dissolution of Li species, which is commonly observed in NASICON type materials. Next, the dissolution rate is controlled by the polymerization of AlO_6 and PO_4 groups, which later triggers secondary phase formation. Our findings are also be applicable to other solution-based methods and can be easily adapted to various NASICON-type materials.

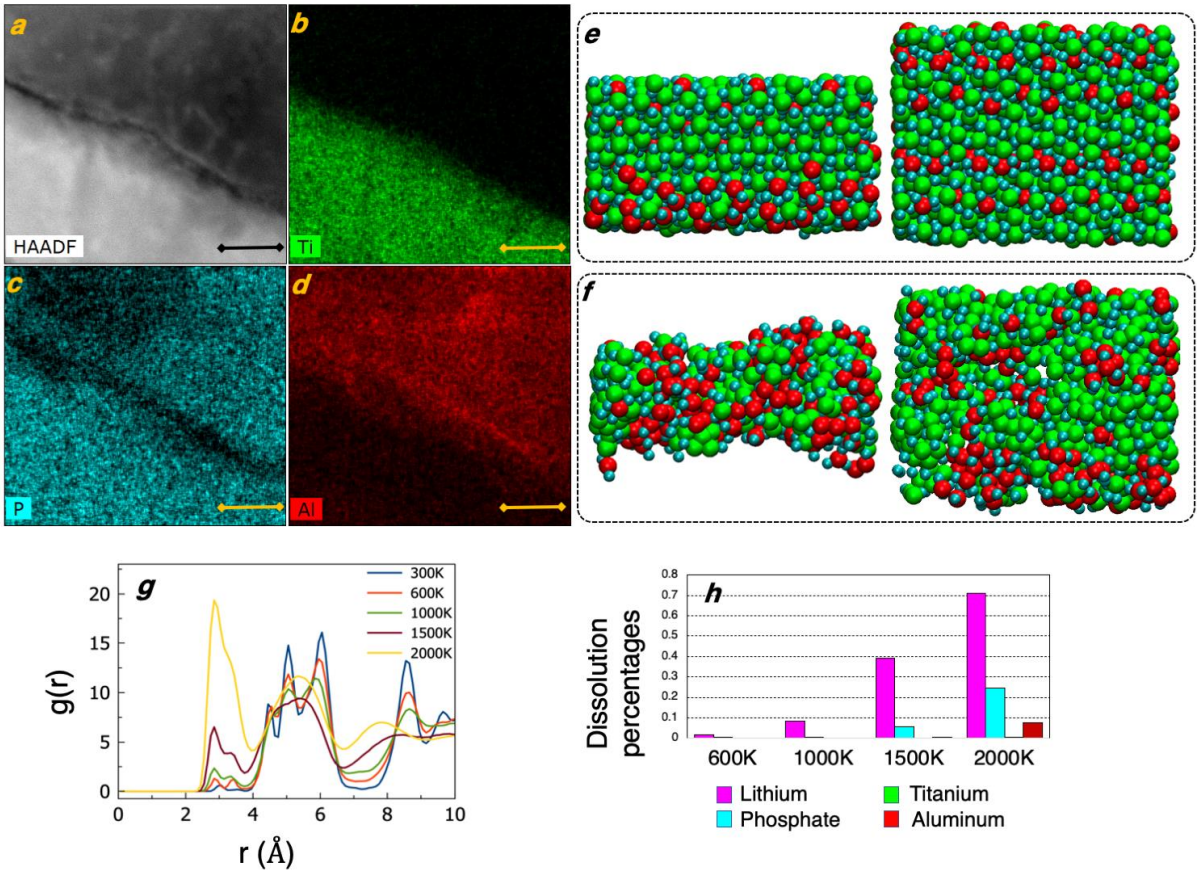

Figure 2. a. HAADF-STEM image with the corresponding **b-d.** STEM-EDS elemental mapping of Al, Ti, and P in a cold sintered sample. EDS mapping images highlight the segregation of Ti and Al, whereas P is homogenously distributed through most of the sample. All the scale bars are 20 nm. **e, f.** Visualization of ReaxFF simulations representing the segregation of Ti and Al. View of LATP slab from two directions before (f) and after (g) dissolution. To increase the visibility of segregation, the liquid phase is not shown. Only Ti, Al, and P are shown for clarity. The structures before dissolution are crystallized with perfect stoichiometry. Key: Ti (green); P (cyan); Al (red). The same colorization is used for TEM images and simulation snapshots. **g.** Evolution of the titanium-titanium radial distribution functions (RDFs) at different temperatures. As the temperature increases, the crystallinity of LATP crystal disappears due to thermal fluctuations until 1000K. After 1500K, a significant change occurs due to dissolved phosphate atoms. **h.** Evolution of the concentration of dissolved Ti, Al, P, and Li species with respect to temperatures.

In this study we iteratively use a combination of experimental observations and computational approaches to investigate the aqueous dissolution of LATP. The densified monolithic palettes were obtained through cold sintering experiments at 130 °C in the presence of water. Details on experimental methods can be found in Methods section. Scanning Electron Microscopy (SEM)

and energy dispersive X-ray spectroscopy (EDS) elemental mapping images for the initial powder (Figure S3 a-d) highlight the homogeneous distribution of phosphorous (P), titanium (Ti) and aluminum (Al) in the initial system. The cations' redistribution is clearly revealed in the cold sintered LATP ceramic using high-angle annular dark-field scanning transmission electron microscopy (HAADF-STEM) combined with EDS elemental mapping as shown in Figure 2a-d. The EDS mapping images demonstrate that Ti segregates in the bottom left grain (Figure 2b) while Al is rich in the top right grain (Figure 2d). In the meantime, P concentration barely varies across the grain boundary (Figure 2c) and has globally a homogenous distribution within the sample. It should be noted that the Al inhomogeneity may even occur within an Al-rich grain (Figure 2d), which is confirmed by Figure S2. Comparing the initial powder and the cold sintered ceramic, one can readily conclude that the observed redistribution of Ti and Al must be a result of incongruent dissolution initiated during the dissolution part of the CSP.

Motivated by our experimental work, we focused on investigating the dissolution dynamics of species at the LATP/water interface. In order to model this interface, molecular dynamics (MD) simulations were conducted using the ReaxFF reactive force field method [22, 23]. The ReaxFF force field used in this work was developed to model LATP/water interfacial reactions [24]. The ReaxFF is capable of simulating sub and supercritical environments [25, 26], which can be assumed to be the state of solvent between grains during CSP due to applied high pressures and elevated temperatures; therefore, ReaxFF was also successfully applied to model CSP surface reaction kinetics at the metal oxide/solvent interfaces [14, 27-30]. Observations of dissolution of chemical species in short simulation time scales (typically nanoseconds) is very unlikely without the usage of accelerated MD methods. However, application of the accelerated methods in such multicomponent systems would not be feasible because all species should be kept freely open to reactions instead of being biased synchronously to drive the dissolution. Instead, we used data from the experimental methods to guide the computational models to mimic experimental conditions. In order to determine the correct dissolved specie concentration kinetics in the simulations, we conducted solubility experiments to measure the dissolution rates for LATP in water (see SI for details, Table S1 and Table S2). The ReaxFF simulations were conducted at high-temperature supercritical conditions. These conditions were established by matching dissolution rates from the simulations with those observed in experiments assuming that the experimental dissolution rates are constant in any region of supercritical state. We monitored the stability of the structure of the connected TiO_6 (AlO_6) and PO_4 polyhedrons to avoid amorphization caused by increased temperatures (see SI for details, Figure S1). Similar to experimental results, the simulations conducted in this work also produced a segregated structure due to incongruent dissolution as shown in Figure 2-e, f.

The LATP has a multicomponent oxide surface that leads to the formation of a large number of oxygen functional groups with different chemical characters; therefore, it has a very complex surface potential. According to our simulations, as soon as water meets with LATP surfaces, some of the water molecules dissociate onto the surface cations and oxygens, while others are adsorbed as molecules to cationic sites. The binding type depends on the adjacent cationic sites and the distance between them. As expected, the protonation of the surface - due to dissociation of water molecules - enables a proton-promoted pathway for the surface dissolution [31]. However, there are additional contributions from the dissolved Li ions. Figure 2h shows the evolution of dissolution concentrations of Li, Al, Ti, and P-based species with temperature. We note that the temperature values in simulations tend to over-estimate exact temperatures due to the relatively short simulated timescales and should be considered not as absolute, but rather an indication of relative trends. According to our simulations, Li dissolution starts at relatively lower temperatures, due to the diffusion channels that are open to the liquid phase in NASICON structure. The Li ions are hydroxylated during the dissolution into the water phase, similar to the predictions reported in the literature ($Li^+ + H_2O \rightarrow LiOH + H^+$) [32]. Our results show that the predominant dissolved Li ion species exists as LiOH at room temperature and make a transition to $Li(OH)_2$ as temperature increases. The $Li(OH)_2$ tends to precipitate on the surface as LiOH. The simulations in this work show that most of the LiOH species bind to surface oxygens adjacent to surface phosphate ions. The bonding of LiOH creates a pathway similar to a proton-promoted dissolution pathway [31]. The bonding between surface oxygen and LiOH polarizes the charge on the oxygen and P, which weakens the bond and makes P available to dissolution. As can be seen in Figure 2h, the dissolution of P follows the increase in Li dissolution and temperature. The first dissolved P at relatively lower temperatures are those that are present on the surface adjacent to LiOH species. In the light of these findings, we can hypothesize that the dissolved Li ions tend to increase the dissolution rate of dominant species on the surface, which in our case are the P-based ions.

The LATP structure consists of a three-dimensional framework with TiO_6 (AlO_6) octahedra and PO_4 tetrahedra connected by sharing an oxygen atom. The framework has a distorted structure, which is stabilized by an equilibrium between the charge distribution on the framework and Li ions. Therefore, it is known that the dissolution of Li ions from the system may affect the rotation of the framework [33]. According to our simulations, the absence of Li ions inside the crystal has additional effects. Figure 3a shows the transition in the bonding between PO_4 and AlO_6 groups. As the radial distribution function (RDF) suggests, the distance between two groups decreases with the increase of temperature. At room temperature, PO_4 groups are bonded to AlO_6 groups in the monodentate form by sharing an oxygen atom. However, with the increase of temperature and the subsequent increase in the dissolution of Li ions, the charge distribution around PO_4 groups changes and they adopt a bidentate binding to AlO_6 groups. This PO_4-AlO_6 bonding transition results in a stable linking between these groups. This stable linkage is one of the reasons behind

the observed incongruency. The monodentate to bidentate transition weakens the connection between AlO_6 and TiO_6 groups and as a result, changes the dissolution rate of Al species. In addition, AlO_6 groups dissolve as a polymerized chain, which further contributes to the increase in the dissolution rate of Al-species (Figure 3b, c, Movie S1). Given that the Al content in crystal and surface is stoichiometrically low compared to Ti, the early dissolution of Al as clusters leaves a Ti-rich crystal behind.

In contrast to what was observed for AlO_6 groups, TiO_6 groups tend to stay in the crystalline state. The TiO_6 groups preserve the bonding structure with PO_4 groups, and the switch from monodentate to bidentate binding similar to AlO_6-PO_4 polymerization has not been observed because as a first-row transition element, Ti atoms have a strong directionality of bonds to oxygens. However, the dissolution of P-based species changes the dynamics for TiO_6 groups. The P-based species tend to dissolve as PO_4 or mostly as PO_3. According to our simulations, PO_4 groups tend to be hydroxylated as ($PO_4^{3-} + 2H_2O \rightarrow H_2PO_4^- + 2OH^-$) while PO_3 groups tend to stay

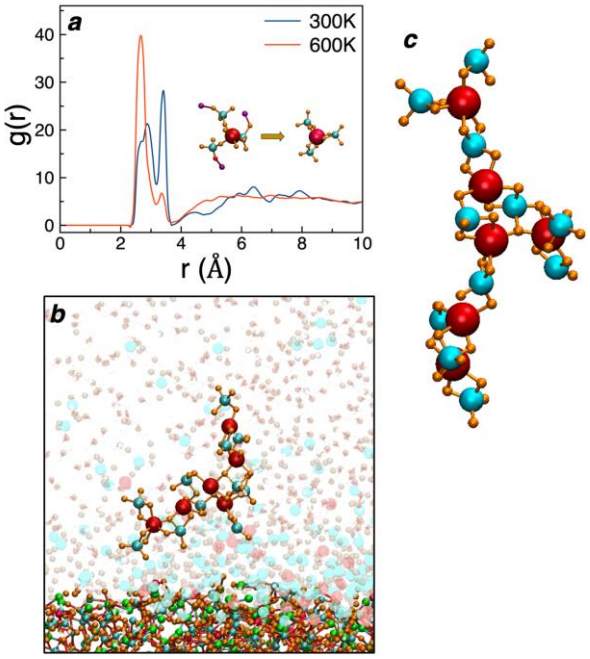

Figure 3. ***a.*** The evolution of the Al-P radial distribution functions with temperature. The blue line represents the room temperature, which is the case when Li ions are inside the crystal. The red line represents increased temperature when Li ion dissolution was initiated. A visual representation of switch between monodentate to bidentate binding of PO_4 group to AlO_6 group is given inside the plot. The visuals are two snapshots from the simulations. Atoms that are not of interest are not shown to increase visibility. ***b.*** A snapshot from the simulations conducted in this work showing the polymerized dissolution of PO_4-AlO_6 groups. To increase visibility, the background liquid phase is represented using blurred colors. ***c.*** A clearer visual representation of the polymerized groups taken from simulations. Key: Ti (green); P (cyan); Al (red); Li (purple); O (orange).

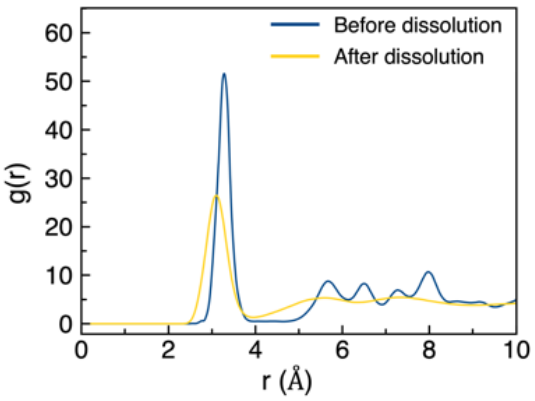

Figure 4. The evolution of the Ti-P radial distribution functions before and after the dissolution of PO_4 groups from the crystal phase. The blue line represents the room temperature, which is the case when PO_4 groups are attached to the structural framework. The yellow line represents a more stable phase between TiO_6 and PO_4 groups due to P-based species dissolution.

unprotonated in the form of a supercritical solution phase. When dissolved, the structural framework loses PO_4 polyhedras, as a result, destabilizes the LATP framework and causes a collapse in some parts, which can be understood from Ti-Ti RDF in Figure 2g. According to our simulations, the collapsed parts initiate conversion to a more stable structure by changing the bonding network between TiO_6 and PO_4 groups, which explains the segregation of Al and Ti species (Figure 2a-d). As can be seen in Ti-P RDF in Figure 4, the distance between these species decreases with the dissolution of PO_3 groups. Also, the loss of PO_4 groups drives a decomposition and forms phase rich in TiO_6, which may initiate growth of secondary phases (e.g., $LiTiOPO_4$, $AlPO_4$) observed in experiments [34, 35].

Conclusions

We conclude by noting that the dissolution of NASICON-type materials can be very complex; however, once better understood, it may be possible to limit incongruent dissolution via smartly designed solutions, for example, by adding electrolyte species to tune dissolution of ions of interest. Our results show that the dissolution of LATP is a sequentially dynamic process. The process starts with the removal of Li ions, which changes the charge distribution inside the crystal. This change triggers a bonding transition inside crystal, which results in dissolution Al as a polymerized AlO_6-PO_4 chains. With the dissolution of PO_3 groups, TiO_6 groups switch to a more stable phase. Our results may be relevant to other NASICON-type materials and may also be of interest to the design of future experiments in solution-based methods.

Author Contributions

The manuscript was written through contributions of all authors. All authors have given approval to the final version of the manuscript.
‡ These authors contributed equally.

Conflicts of interest

There are no conflicts to declare

Acknowledgements

ACTvD acknowledges funding support from the Multi-Scale Fluid-Solid Interactions in Architected and Natural Materials (MUSE) Center funded by U.S. Department of Energy (DOE). C.R. acknowledges partial funding support from the Air Force Office of Scientific Research under Award No. FA9550-16-1-0429. M.Y.S. acknowledges partial funding support from U.S. National Science Foundation under Award No. DMR-1842922. The work presented herein was funded in part by the Advanced Research Projects Agency-Energy, U.S. DOE, under Award No. DE-AR0000766.

Notes and references

1. He, X.; Zhu, Y.; Mo, Y., Origin of fast ion diffusion in super-ionic conductors. *Nat Commun* **2017,** *8*, 15893.
2. Manthiram, A.; Yu, X.; Wang, S., Lithium battery chemistries enabled by solid-state electrolytes. *Nature Reviews Materials* **2017,** *2* (4).
3. Famprikis, T.; Canepa, P.; Dawson, J. A.; Islam, M. S.; Masquelier, C., Fundamentals of inorganic solid-state electrolytes for batteries. *Nat Mater* **2019**.
4. Murugan, R.; Thangadurai, V.; Weppner, W., Fast lithium ion conduction in garnet-type Li(7)La(3)Zr(2)O(12). *Angew Chem Int Ed Engl* **2007,** *46* (41), 7778-81.
5. Li, Y.; Xu, H.; Chien, P. H.; Wu, N.; Xin, S.; Xue, L.; Park, K.; Hu, Y. Y.; Goodenough, J. B., A Perovskite Electrolyte That Is Stable in Moist Air for Lithium-Ion Batteries. *Angew Chem Int Ed Engl* **2018,** *57* (28), 8587-8591.
6. Ma, F.; Zhao, E.; Zhu, S.; Yan, W.; Sun, D.; Jin, Y.; Nan, C., Preparation and evaluation of high lithium ion conductivity Li 1.3 Al 0.3 Ti 1.7 (PO 4) 3 solid electrolyte obtained using a new solution method. *Solid State Ionics* **2016,** *295*, 7-12.
7. Han, F.; Yue, J.; Chen, C.; Zhao, N.; Fan, X.; Ma, Z.; Gao, T.; Wang, F.; Guo, X.; Wang, C., Interphase Engineering Enabled All-Ceramic Lithium Battery. *Joule* **2018,** *2* (3), 497-508.
8. Berbano, S. S.; Guo, J.; Guo, H.; Lanagan, M. T.; Randall, C. A., Cold sintering process of Li1.5Al0.5Ge1.5(PO4)3 solid electrolyte. *Journal of the American Ceramic Society* **2017,** *100* (5), 2123-2135.
9. Kunshina, G. B.; Gromov, O. G.; Lokshin, E. P.; Kalinnikov, V. T., Sol-gel synthesis of Li1.3Al0.3Ti1.7(PO4)(3) solid electrolyte. *Russ J Inorg Chem+* **2014,** *59* (5), 424-430.
10. Kotobuki, M.; Koishi, M., Preparation of Li1.5Al0.5Ti1.5(PO4)(3) solid electrolyte via a sol-gel route using various Al sources. *Ceram Int* **2013,** *39* (4), 4645-4649.
11. Kim, K. M.; Shin, D. O.; Lee, Y. G., Effects of preparation conditions on the ionic conductivity of hydrothermally synthesized Li1+xAlxTi2-x(PO4)(3) solid electrolytes. *Electrochim Acta* **2015,** *176*, 1364-1373.
12. Rosenberger, A.; Gao, Y.; Stanciu, L., Field-assisted sintering of Li 1.3 Al 0.3 Ti 1.7 (PO 4) 3 solid-state electrolyte. *Solid State Ionics* **2015,** *278*, 217-221.
13. Guo, J.; Guo, H.; Baker, A. L.; Lanagan, M. T.; Kupp, E. R.; Messing, G. L.; Randall, C. A., Cold Sintering: A Paradigm Shift for Processing and Integration of Ceramics. *Angew Chem Int Ed Engl* **2016,** *55* (38), 11457-61.
14. Sengul, M. Y.; Guo, J.; Randall, C. A.; van Duin, A. C. T., Water-Mediated Surface Diffusion Mechanism Enables the Cold Sintering Process: A Combined Computational and Experimental Study. *Angew Chem Int Ed Engl* **2019,** *58* (36), 12420-12424.
15. Lee, W.; Lyon, C. K.; Seo, J. H.; Lopez-Hallman, R.; Leng, Y.; Wang, C. Y.; Hickner, M. A.; Randall, C. A.; Gomez, E. D., Ceramic–Salt Composite Electrolytes from Cold Sintering. *Adv Funct Mater* **2019,** *29* (20).
16. Seo, J.-H.; Guo, J.; Guo, H.; Verlinde, K.; Heidary, D. S. B.; Rajagopalan, R.; Randall, C. A., Cold sintering of a Li-ion cathode: LiFePO4-composite with high volumetric capacity. *Ceram Int* **2017,** *43* (17), 15370-15374.
17. Berbano, S. S.; Guo, J.; Guo, H.; Lanagan, M. T.; Randall, C. A., Cold sintering process of Li1.5Al0.5Ge1.5(PO4)3 solid electrolyte. *J. Am. Ceram. Soc.* **2017,** *100* (5), 2123-2135.
18. Guo, J.; Berbano, S. S.; Guo, H.; Baker, A. L.; Lanagan, M. T.; Randall, C. A., Cold Sintering Process of Composites: Bridging the Processing Temperature Gap of Ceramic and Polymer Materials. *Adv. Funct. Mater.* **2016,** *26* (39), 7115-7121.
19. Guo, J.; Legum, B.; Anasori, B.; Wang, K.; Lelyukh, P.; Gogotsi, Y.; Randall, C. A., Cold Sintered Ceramic Nanocomposites of 2D MXene and Zinc Oxide. *Adv Mater* **2018,** *30* (32), e1801846.
20. Fuentes, R. O.; Figueiredo, F.; Marques, F. M. B.; Franco, J. I., Reaction of NASICON with water. *Solid State Ionics* **2001,** *139* (3-4), 309-314.
21. Rustad, J. R.; Casey, W. H., Metastable structures and isotope exchange reactions in polyoxometalate ions provide a molecular view of oxide dissolution. *Nat Mater* **2012,** *11* (3), 223-6.
22. van Duin, A. C. T.; Dasgupta, S.; Lorant, F.; Goddard, W. A., ReaxFF: A reactive force field for hydrocarbons. *Journal of Physical Chemistry A* **2001,** *105* (41), 9396-9409.
23. Senftle, T. P.; Janik, M. J.; van Duin, A. C. T., A ReaxFF Investigation of Hydride Formation in Palladium Nanoclusters via Monte Carlo and Molecular Dynamics Simulations. *J Phys Chem C* **2014,** *118* (9), 4967-4981.
24. Shin, Y. K.; Sengul, M. Y.; Jonayat, A. S. M.; Lee, W.; Gomez, E. D.; Randall, C. A.; Duin, A., Development of a ReaxFF reactive force field for lithium ion conducting solid electrolyte Li1+xAlxTi2-x(PO4)3 (LATP). *Phys Chem Chem Phys* **2018,** *20* (34), 22134-22147.
25. Sengul, M. Y.; Randall, C. A.; van Duin, A. C. T., ReaxFF molecular dynamics simulation of intermolecular structure formation in acetic acid-water mixtures at elevated temperatures and pressures. *J Chem Phys* **2018,** *148* (16), 164506.
26. Manzano, H.; Zhang, W.; Raju, M.; Dolado, J. S.; Lopez-Arbeloa, I.; van Duin, A. C. T., Benchmark of ReaxFF force field for subcritical and supercritical water. *J Chem Phys* **2018,** *148* (23), 234503.
27. Sengul, M. Y.; Randall, C. A.; van Duin, A. C. T., ReaxFF Molecular Dynamics Study on the Influence of Temperature on Adsorption, Desorption, and Decomposition at the Acetic Acid/Water/ZnO(1010) Interface Enabling Cold Sintering. *ACS Appl Mater Interfaces* **2018,** *10* (43), 37717-37724.
28. Ndayishimiye, A.; Sengul, M. Y.; Akbarian, D.; Fan, Z.; Tsuji, K.; Bang, S. H.; van Duin, A. C. T.; Randall, C. A., Dynamics of the Chemically Driven Densification of Barium Titanate Using Molten Hydroxides. *Nano Lett* **2021,** *21* (8), 3451-3457.
29. Ndayishimiye, A.; Sengul, M. Y.; Bang, S. H.; Tsuji, K.; Takashima, K.; Hérisson de Beauvoir, T.; Denux, D.; Thibaud, J.-M.; van Duin, A. C. T.; Elissalde, C.; Goglio, G.; Randall, C. A., Comparing hydrothermal sintering and cold sintering process:

Mechanisms, microstructure, kinetics and chemistry. *Journal of the European Ceramic Society* **2020,** *40* (4), 1312-1324.
30. Ndayishimiye, A.; Sengul, M. Y.; Sada, T.; Dursun, S.; Bang, S. H.; Grady, Z. A.; Tsuji, K.; Funahashi, S.; van Duin, A. C. T.; Randall, C. A., Roadmap for densification in cold sintering: Chemical pathways. *Open Ceramics* **2020,** *2*.
31. Stumm, W., Chemistry of the solid-water interface : processes at the mineral-water and particle-water interface in natural systems. Sigg, L.; Sulzberger, B., Eds.
32. Veerman, A.; Lee, H. M.; Kim, K. S., Dissolution nature of the lithium hydroxide by water molecules. *J Chem Phys* **2005,** *123* (8), 084321.
33. Alamo, J., Chemistry and Properties of Solids with the [Nzp] Skeleton. *Solid State Ionics* **1993,** *63-5*, 547-561.
34. DeWees, R.; Wang, H., Synthesis and Properties of NaSICON-type LATP and LAGP Solid Electrolytes. *ChemSusChem* **2019,** *12* (16), 3713-3725.
35. Hupfer, T.; Bucharsky, E. C.; Schell, K. G.; Hoffmann, M. J., Influence of the secondary phase LiTiOPO 4 on the properties of Li 1+x Al x Ti 2−x (PO 4) 3 (x = 0; 0.3). *Solid State Ionics* **2017,** *302*, 49-53.